Influence of Al^{3+} doping on the energy levels and thermal property of the $3.5MgO{\cdot}0.5MgF_2{\cdot}GeO_2{:}Mn^{4+}$ red-emitting phosphor*

Yuan Lin-lin(苑琳琳), Zhang Xiao-Song(张晓松), Xu Jian-Ping(徐建萍), Sun Jian(孙 健), Jin Han(金 含), Liu Xiao-Juan(刘晓娟), Li Lin-Lin(李霖霖), and Li Lan(李 岚)†

Institute of Material Physics, Key Laboratory for Optoelectronic Materials and Devices of Tianjin, Key Laboratory of Display Materials and Photoelectric Devices of Ministry of Education, Tianjin University of Technology, Tianjin 300384, *China*

(Received 21 January 2015; revised manuscript received 19 March 2015; published online 20 June 2015)

A series of Al^{3+}-doped $3.5MgO{\cdot}0.5MgF_2{\cdot}GeO_2{:}Mn^{4+}$ red-emitting phosphors is synthesized by high temperature solid-state reaction. The broad excitation band at 300 nm–380 nm, resulting from the $^4A_2 \rightarrow {}^4T_1$ transition of Mn^{4+}, exhibits a blue shift with the increase of Al_2O_3 content. The observation of the decreased Mn^{4+}–O^{2-} distance is explained by the crystal field theory. The temperature-dependent photoluminescence spectra with various amounts of Al_2O_3 content are comparatively measured and the calculation shows that the activation energy increases up to 0.41 eV at the Al_2O_3 content of 0.1 mol. The maximum phonon densities of state for these samples are calculated from Raman spectra and they are correlated with the thermal properties.

Keywords: phosphors, photoluminescence, thermal properties

PACS: 78.55.–m, 33.50.–j, 65.40.–b **DOI:** 10.1088/1674-1056/24/8/087802

1. Introduction

With high energy conversion efficiency, low energy consumption, long lifetime, and environment-friendly, white light-emitting diodes (WLEDs) have stimulated the development of solid-state lighting technology.[1] In most commercial WLED devices with a typical internal structure, including blue GaN chip and yellow emitting YAG:Ce^{3+} phosphor, the low red emission intensity of YAG:Ce^{3+} phosphors gives rise to the poor color rendering index (CRI) and higher correlated color temperature. The one possible solution was found to adopt trichromatic phosphors combining the near-UV (NUV) LED chips.[2,3] In addition, the high emission efficiency and thermally stable red-emitting phosphors are necessary to lower the thermal quenching at the high operating temperature (up to 425 K) of chips.[4]

Currently, the selected red-emitting phosphors for WLEDs are focused on nitrides- and sulfide-based compounds with activated centers, such as rare-earth ions[2–6] and transition metal ions.[7–9] Eu^{2+}-doped nitride phosphors with high color rendering indexes are regarded as good candidate red-emitting phosphors for WLEDs under UV or blue chip excitation.[2–4] However, synthesis conditions are required, including high reaction temperature and the high pressure N_2 gas. Although the higher emission efficiency from sulfide red-emitting phosphor, such as $(Ca_{1-x},Sr_x)S{:}Eu^{2+}$,[5] has been achieved,[6] the poor thermal stability and sensitivity to moisture may restrict the stability and lifetime of the device. Mn^{4+}-activated dialkali hexafluorometallate hosts, such as $BaSiF_6$,[7] $ZnSiF_6$,[8] and K_2SiF_6,[9] are found to match well with the emission wavelength of InGaN chip and can achieve highly efficient red luminescence.

It is generally considered that energy level structure and electronic transition probability of luminescence centers are highly interrelated with the crystal field strength of the ligands.[10] Bachmannet *et al.*[2] found a red-shift in the Eu^{2+} emission band when replacing part of Sr^{2+} ions by Ca^{2+} ions in the host of $SrSi_2O_2N_2$. They suggested that an increased crystal field splitting lowered the energy difference between 5d–4f state of Eu^{2+}. Dai *et al.*[10] investigated the PL spectra of Eu^{2+}-doped $KSrPO_4$ when substituting part of K^+ cations by Na^+ cations in the host. A red-shift in 430-nm band was attributed to the shift of Eu^{2+} 5d energy level which was influenced by contraction and distortion of the unit cell. As the feature of the outside 3d electrons,[11] the energy level of transition metal ions are much affected by the crystal field strength of the matrix.[12] For Mn^{4+}-activated $Ln_2Sn_2O_7$ (Ln = Lu^{3+}, Y^{3+}, and Gd^{3+}), the increased Mn^{4+}–O^{2-} bond length induced the decrease in crystal field strength and energy level difference between $^4A_2$ and $^4T_2$.[13]

In consideration of the formation of stable polyhedron structure, Al^{3+} co-doping has a significant role in crystal field strength and luminescence properties.[14–16] The increase of Al^{3+} addition in $ZnGa_2O_4{:}Cr^{3+}$ induced a blue-shift of the excitation spectra due to the increase of crystal field strength.[17] The deep red luminescence of the Mn^{4+}

*Project supported by the National High Technology Research and Development Program of China (Grant No. 2013AA014201), the Natural Science Foundation of Tianjin City, China (Grant Nos. 11JCYBJC00300 and 14JCZDJC31200), and the National Key Foundation for Exploring Scientific Instrument of China (Grant No. 2014YQ120351).

†Corresponding author. E-mail: lilan@tjut.edu.cn

© 2015 Chinese Physical Society and IOP Publishing Ltd

ion in $3.5MgO{\cdot}0.5MgF_2{\cdot}GeO_2$, which was derived by replacing part of MgO in $4MgO{\cdot}GeO_2$ with MgF_2, had given rise to an increasing luminescence intensity.[18,19] In addition, the two broad excitation bands in a range of 300 nm–480 nm make it suitable for UV and blue LED chips. In this paper, $3.5MgO{\cdot}0.5MgF_2 \cdot (1-2x)GeO_2 \cdot xAl_2O_3{:}0.01Mn^{4+}$ ($0 \leq x \leq 0.15$ mol) phosphors are synthesized by the high temperature solid-state reaction method. The influence of foreign Al^{3+} ions on energy levels of the Mn^{4+} ions and thermal properties of phosphors are also discussed.

2. Experiment

Powder samples were prepared by the high temperature solid-state reaction of mixtures with appropriate molar ratios for $3.5MgO{\cdot}0.5MgF_2 \cdot (1-2x)GeO_2 \cdot xAl_2O_3{:}0.01Mn^{4+}$ ($0 \leq x \leq 0.15$ mol) with starting materials consisting of MgO, MgF_2 of 99.9% purity, GeO_2, Al_2O_3 of 99.999% purity, and MnO_2 of 99.99% purity. The mixture was thoroughly mixed and transferred to a corundum crucible, which was heated at 1100 °C for 6 h under atmosphere. After cooling to room temperature, the as-prepared samples were completely ground.

The crystal structures of powder samples were characterized by using a Rigaku 2500/PC x-ray diffractometer (XRD) with Cu Kα radiation source (0.1542 nm) at 40 kV and 150 mA. The scanning electron microscope (SEM) images and energy dispersive spectroscopy (EDS) spectra were obtained by field emission scanning electron microscopy (FESEM, HITACHI SU8010). Photoluminescence (PL) and excitation (PLE) measurements were performed by Jobin Yvon FL3 fluorescence spectrophotometer with a 450-W xenon lamp as an excitation source. Temperature-dependent PL spectra were measured at temperatures ranging from 300 K to 540 K by the same spectrophotometer with home-made heating equipment. Raman spectra were recorded using a RENISHAW InVia Raman microscope and an argon ion laser operating at 785 nm. All of the measurements were carried out in ambient atmosphere.

3. Results and discussion

The XRD patterns for phosphor samples are revealed in Fig. 1. The samples each have an $Mg_{28}Ge_{10}O_{48}$-like structure that belongs to orthorhombic symmetry with space group *Pbam* and cell parameters $a = 14.343$ Å, $b = 10.196$ Å, and $c = 5.908$ Å, which were reported by Von Dreele *et al.*[20] and Bless *et al.*[21] No diffraction peak shift is observed in any of the samples with different doping amounts of Al^{3+}. Considering the ion valence state and electro-negativity, Ge^{4+} could be substituted by Al^{3+} ions to keep the electric neutrality by substituting F^- into O^{2-} sites.[21,22] For similar effective ionic radii of Ge^{4+} ($r = 0.39$ Å, $CN = 4$) and Al^{3+} ($r = 0.39$ Å, $CN = 4$), Al^{3+} substituted in host lattice can be determined as no detectable change in cell volume. The SEM images and EDS spectra for the as-prepared phosphors at Al_2O_3 concentrations of 0, 0.05, 0.1, and 0.15 mol are shown in Fig. 2. Similar particle morphologies of polyhedra and sizes are observed for all of the samples. The atomic ratios for all cations in samples, which are summarized in Table 1, are consistent with the molar ratios of raw materials.

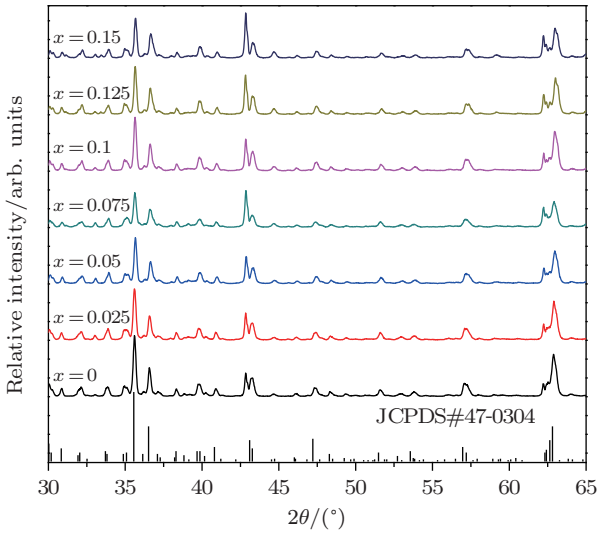


Fig. 1. (color online) The XRD patterns for the $3.5MgO{\cdot}0.5MgF_2 \cdot (1-2x)GeO_2 \cdot xAl_2O_3{:}0.01Mn^{4+}$ ($0 \leq x \leq 0.15$ mol) phosphors.

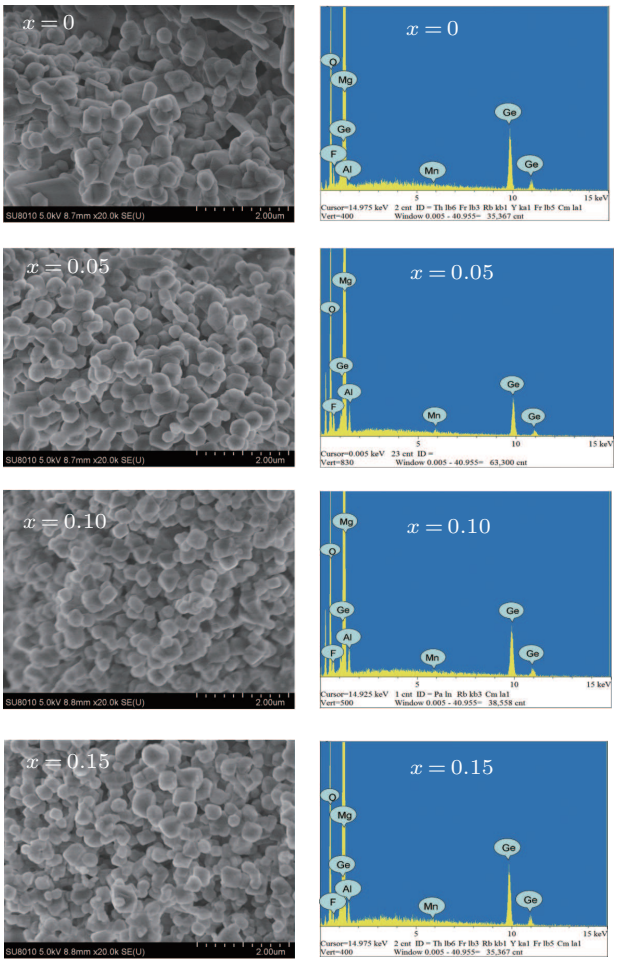


Fig. 2. (color online) The SEM images and EDS spectra of the samples at Al_2O_3 content values of 0, 0.05, 0.1, and 0.15 mol.

Table 1. Atomic ratios of all elements doped with different amounts of Al_2O_3.

Al_2O_3 content/mol	O/at.%	F/at.%	Mg/at.%	Mn/at.%	Ge/at.%	Al/at.%
0	47.816	8.68	34.711	0.082	8.705	0.006
0.05	47.632	8.752	34.812	0.087	7.846	0.871
0.1	47.398	8.774	34.998	0.084	6.988	1.758
0.15	47.174	8.765	35.101	0.082	6.198	2.68

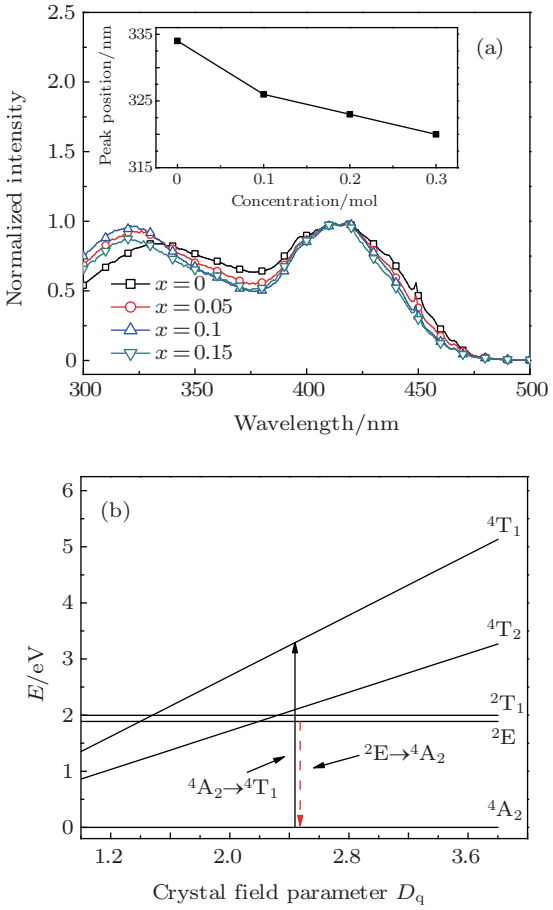


Fig. 3. (color online) (a) Normalized PLE spectra of the samples with Al_2O_3 content values of 0, 0.05, 0.1, and 0.15 mol for the 657-nm emission of Mn^{4+}. The inset shows the variation of peak position for wavelength band 300 nm–380 nm with Al^{3+} concentration. (b) The energy level diagram for the d^3 configuration.

The PLE spectra of $3.5MgO{\cdot}0.5MgF_2 \cdot (1-2x)GeO_2 \cdot xAl_2O_3{:}0.01Mn^{4+}$ ($x = 0$, 0.05, 0.1, and 0.15 mol) are shown in Fig. 3(a). The two broad wavelength ranges of 300 nm–380 nm and 380 nm–480 nm correspond to the spin-allowed $^4A_2 \rightarrow {}^4T_1$ and $^4A_2 \rightarrow {}^4T_2$ transitions of Mn^{4+} ions, respectively.[18,19] The higher-energy band peak shows the blue-shift from 334 nm to 320 nm with the increase of Al^{3+} concentration, whereas the lower-energy excitation band has no obvious change. As described by Von Dreele *et al.*[20] and Bless *et al.*,[21] Mg^{2+} ions occupied the center of the octahedral coordination sites by six oxygen atoms with two different Mg^{2+}–O^{2-} bond distances. And Mn^{4+} ions were suggested to occupy Mg^{2+} sites of the center octahedral symmetry.[22] The bond distance calculated by Vienna *ab-initio* simulation package (VASP) is 2.164 Å for Mn^{4+}–O_{I}^{2-} and 2.091 Å for Mn^{4+}–O_{Π}^{2-} without Al_2O_3 incorporated, which are slightly larger than 2.158 Å and 2.086 Å for the Al_2O_3-doped structure, respectively. According to the Tanabe–Sugano energy diagram of d^3 coordination in Fig. 3(b), the excitation energy between the ground state $^4A_2$ and the excited state $^4T_1/{}^4T_2$ is strongly related to the crystal field strength, and their relationship can be expressed as[23,24]

$$D_{\mathrm{q}} = \frac{3Ze^2r^4}{5R^5}, \tag{1}$$

where D_{q} is the crystal field strength for octahedral symmetry, R is the distance between the central ion and its ligand, Z is the charge or valence of the anion, e is the charge of the electron, and r is the radius of the d-wave function. The increased crystal field strength from shortened Mn^{4+}–O^{2-} bond distance in the six-fold coordination brings about the shifts of $^4T_1$ and $^4T_2$ energy levels of Mn^{4+}, resulting in the observed blue-shift of $^4A_2 - {}^4T_1$ excitation band.

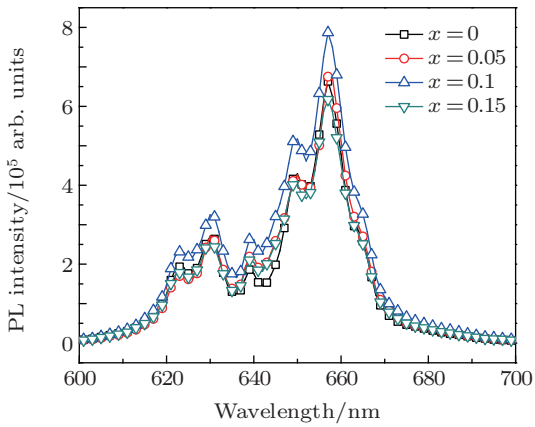


Fig. 4. (color online) The PL spectra of the $3.5MgO{\cdot}0.5MgF_2 \cdot (1-2x)GeO_2 \cdot xAl_2O_3{:}0.01Mn^{4+}$ phosphors with Al_2O_3 concentrations of $x = 0$, 0.05, 0.1, and 0.15 mol.

Figure 4 shows the PL spectra of $3.5MgO{\cdot}0.5MgF_2 \cdot (1-2x)GeO_2 \cdot xAl_2O_3{:}0.01Mn^{4+}$ phosphors with different Al_2O_3 concentrations of 0, 0.05, 0.1, and 0.15 mol. There are five sharp red emission peaks located at 623, 630, 639, 649, and 657 nm, respectively, which is ascribed to the different vibrational modes of $^2E \rightarrow {}^4A_2$ of Mn^{4+} ions. The two dominant peaks around 649 nm and 657 nm originate from Stokes vibrational band by the coupling of the asymmetric Mn^{4+}–O^{2-} deformation and stretching modes.[19,22] Since the $^2E \rightarrow {}^4A_2$ transition is spin- and parity-forbidden, the two weak emission bands from the anti-Stokes can be observed at around 623 nm and 630 nm. And the peak at 639 nm, which seems to be

weakest, is from the zero-phonon transition.[19,22] Owing to their weak dependence on crystal field strength, the emission peaks for ^{2}E energy level are almost unchanged.

A main obstacle in developing practical WLED technology is the thermal quenching of phosphors; i.e., the luminescent efficiency and color rendering index deteriorate with an increase of the operating temperature. Figure 5 shows the PL emission spectra of $3.5MgO{\cdot}0.5MgF_2 \cdot (1-2x)GeO_2 \cdot xAl_2O_3{:}0.01Mn^{4+}$ ($x = 0$, 0.05, 0.1, and 0.15 mol) phosphors under 400-nm excitation in a temperature range from 300 K to 540 K. Their main emission peak positions are kept at 657 nm for all samples, whereas the full width at half maximum (FWHM) is obviously broadened with the increase of the measurement temperature as shown in Fig. 6(a). This phenomenon is associated with the enhanced electron–phonon interaction by the increased population density of phonons at high temperature.[25] The normalized emission intensities under different measurement temperatures are displayed in Fig. 6(b).

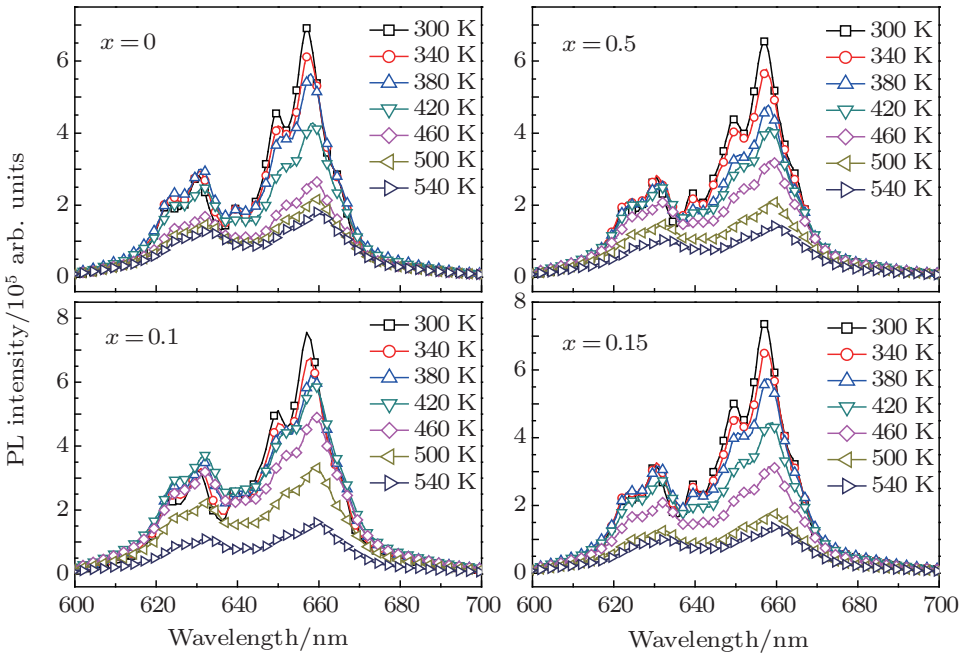


Fig. 5. (color online) Temperature-dependent PL spectra of phosphors with Al_2O_3 concentration $x = 0$, 0.05, 0.1, and 0.15 mol under the excitation of 400 nm.

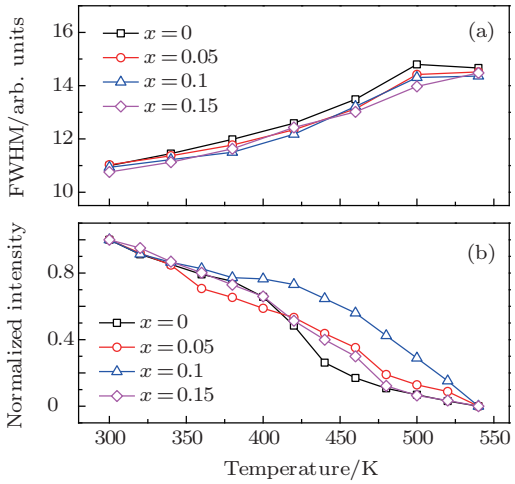


Fig. 6. (color online) Temperature-dependence of (a) FWHMs and (b) normalized emission intensities of the $3.5MgO{\cdot}0.5MgF_2 \cdot (1-2x)GeO_2 \cdot xAl_2O_3{:}0.01Mn^{4+}$ phosphors with $x = 0$, 0.05, 0.1, and 0.15 mol.

As the temperature increases from room temperature up to 425 K, the emission intensities reach 45.7%, 49.8%, 72.5%, and 52.3% of initial intensity for $x = 0$, 0.05, 0.1, and 0.15 mol, respectively. The activation energy can be determined with fitting procedure by using the Arrhenius equation,[25,26]

$$I_T = I_0/[1 + c\exp(-\Delta E/kT)], \tag{2}$$

where I_0 is the initial intensity, I_T is the intensity at a given

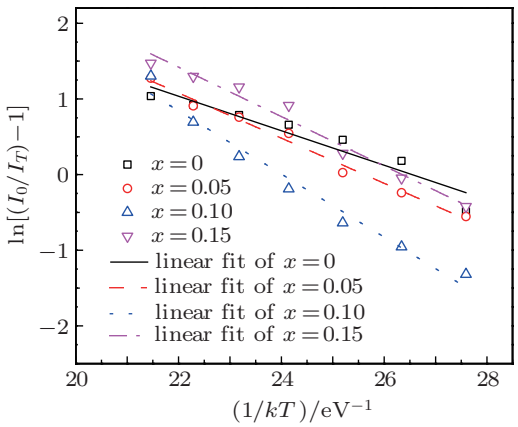


Fig. 7. (color online) Fitted curves for $\ln[(I_0/I_T)-1]$ versus $1/kT$ from Arrhenius equation. The symbols and straight lines represent the experimental data and fitted line under Al_2O_3 concentrations of 0, 0.05, 0.1, 0.15 mol, respectively.

temperature T, c is a constant for a certain host, ΔE is the activation energy for thermal quenching, and k is the Boltzmann's constant. The thermal quenching data under different Al_2O_3 concentrations in Fig. 6(b) are fitted for the curves in Fig. 7. The slope values, which are indicated as ΔE, are 0.23, 0.30, 0.41, and 0.33 eV, respectively.

The nonradiative transition process at high temperature is usually associated with the enhanced electron–phonon interaction due to the increased population density of phonons.[25,26] The influence of Al^{3+} doping on the phonon energy of $3.5MgO{\cdot}0.5MgF_2{\cdot}GeO_2$ is discussed according to Raman spectra in Fig. 8. Except for the band of octahedral MnO_6[27] and tetrahedral GeO_4 group,[28,29] the emerging band at 702 cm^{-1} for Al_2O_3 doping samples is ascribed to the stretching vibration of tetrahedral AlO_4 groups.[30,31] It was suggested in Refs. [23] and [32] that the nonradiative relaxation probability can be described by $W_{NP} = C[n(T)+1]^P \exp(-\alpha\Delta E)$, in which constant C is dependent on the phonon density of state $\rho(\omega_P)$[33] and expressed as $C \propto \rho(\omega)^{5/3}$. The maximum phonon density of state $\rho_m(\omega_P)$ is typically described as the integral area ratio of the band at 827 cm^{-1}–867 cm^{-1}, corresponding to maximum phonon energy, to the whole band of the Raman spectrum. The values of $\rho_m(\omega_P)$ are calculated to be 0.1086, 0.1081, 0.0804, and 0.1051 for Al_2O_3 concentration $x = 0$, 0.05, 0.1, and 0.15 mol, respectively. The minimum value of $\rho_m(\omega_P)$ at 0.1-mol Al_2O_3 doping is consistent with the observed weak thermal quenching.

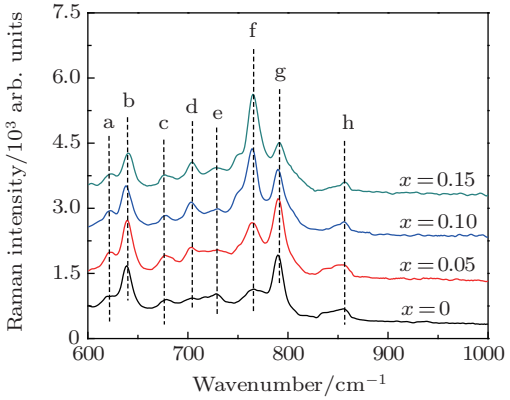


Fig. 8. (color online) Raman spectra for Al_2O_3 content values of 0, 0.05, 0.1, and 0.15 mol at room temperature. The bands denoted as a and b are the asymmetric stretching modes of octahedral MnO_6. The band d is due to the stretching vibration of tetrahedral AlO_4. The symmetric stretching, antisymmetric stretching, and stretching vibration modes of tetrahedral GeO_4 are assigned to c, f, g, e, and h, respectively.

4. Conclusions

In this work, we synthesize a series of red-emission Mn^{4+}-activated $3.5MgO{\cdot}0.5MgF_2 \cdot (1-2x)GeO_2 \cdot xAl_2O_3{:}0.01Mn^{4+}$ ($0 \le x \le 0.15$ mol) phosphors by high temperature solid-state reaction. The phosphors each exhibit a strong red emission under UV light excitation. The broad excitation band in 300 nm–380 nm, which originates from the $^4A_2 \rightarrow {}^4T_1$ transition of Mn^{4+}, is observed to be blue-shifted with the increase of addition Al_2O_3. We conclude that the crystal field strength D_q of the octahedral lattice structure could be changed by Al^{3+} additive due to the variation of Mn^{4+}–O^{2-} bond length. Temperature-dependent PL spectra are measured in a temperature range of 300 K–540 K. The thermal stability is found to be optimal for 0.1 mol of Al^{3+} doping concentration with the activation energy of 0.41 eV. The maximum phonon density of state is used to explain the thermal quenching effect.

References

[1] Dong X, Zhang J, Zhang X, Hao Z and Luo Y 2014 *J. Alloys Compd.* **587** 493
[2] Bachmann V, Ronda C, Oeckler O, Schnick W and Meijerink A 2009 *Chem. Mater.* **21** 316
[3] Suehiro T, Xie R J and Hirosaki N 2013 *Ind. Eng. Chem. Res.* **52** 7453
[4] Xie R J, Hirosaki N, Suehiro T, Xu F F and Mitomo M 2006 *Chem. Mater.* **18** 5578
[5] Jia D and Wang X 2007 *Opt. Mater.* **30** 375
[6] Wu Y C, Chen Y C, Wang D Y, Lee C S, Sun C C and Chen T M 2011 *J. Mater. Chem.* **21** 15163
[7] Sekiguchi D, Nara J and Adachi S 2013 *J. Appl. Phys.* **113** 183516
[8] Hoshino R and Adachi S 2013 *J. Appl. Phys.* **114** 213502
[9] Lv L, Jiang X, Huang S, Chen X and Pan Y 2014 *J. Mater. Chem. C* **2** 3879
[10] Dai P, Zhang X, Bian L, Lu S, Liu Y and Wang X 2013 *J. Mater. Chem. C* **1** 4570
[11] Orgel L E 1955 *J. Chem. Phys.* **23** 1004
[12] Du M H 2014 *J. Mater. Chem. C* **2** 2475
[13] Srivastava A M and Brik M G 2012 *Opt. Mater.* **35** 196
[14] Peng M, Yin X, Tanner P A, Liang C, Li P, Zhang Q and Qiu J 2013 *J. Am. Ceram. Soc.* **96** 2870
[15] Park K, Kim J and Kim K Y 2012 *Mater. Chem. Phys.* **136** 264
[16] Atabaev T S, Thi Vu H H, Piao Z, Hwang Y H and Kim H K 2012 *J. Alloys Compd.* **541** 263
[17] Zhang W, Zhang J, Chen Z, Wang T and Zheng S 2010 *J. Lumin.* **130** 1738
[18] Thorington L 1950 *J. Opt. Soc. Am.* **40** 579
[19] Shao Q, Lin H, Hu J, Dong Y and Jiang J 2013 *J. Alloys Compd.* **552** 370
[20] Von Dreele R B, Bless P W, Kostiner E and Hughes R E 1970 *J. Solid State Chem.* **2** 612
[21] Bless P W, Von Dreele R B, Kostiner E and Hughes R E 1972 *J. Solid State Chem.* **4** 262
[22] Okamoto S and Yamamoto H 2010 *J. Electrochem. Soc.* **157** 59
[23] Kuo T W, Liu W R and Chen T M 2010 *Opt. Express* **18** 1888
[24] Brgoch J, Borg C K H, Denault K A, Mikhailovsky A, DenBaars S P and Seshadri R 2013 *Inorg. Chem.* **52** 8010
[25] Xia Z, Wang X, Wang Y, Liao L and Jing X 2011 *Inorg. Chem.* **50** 10134
[26] Xu S Y, Zhang X S, Zhou Y L, Xi Q and Li L 2011 *Chin. Phys. B* **20** 037804
[27] Granado E, Moreno N O, García A, Sanjurjo J A, Rettori C, Torriani I, Oseroff S B, Neumeier J J, McClellan K J, Cheong S W and Tokura Y 1998 *Phys. Rev. B* **58** 11435
[28] Guyot F, Boyer H, Madon M, Velde B and Poirier J P 1986 *Phys. Chem. Minerals* **13** 91
[29] Mamiya S 2013 *Mod. Appl. Sci.* **7** 22
[30] Chah K, Boizot B, Reynard B, Ghaleb D and Petite G 2002 *Nucl. Instrum. Method Phys. Res. B* **191** 337
[31] Merzbacher C I and White W B 1991 *J. Non-Cryst. Solids* **130** 18
[32] Zhou Y L, Zhang X S, Xu J P, Zhang Z P, Zhang G F, Wei F W and Li L 2012 *Chin. Phys. B* **21** 066301
[33] Layne C B, Lowdermilk W H and Weber M J 1977 *Phys. Rev. B* **16** 10